Draft version August 15, 2013
Preprint typeset using LaTeX style emulateapj v. 11/10/09

ON MEASURING INNER HALO PROFILES WITH WEAK LENSING SHEAR AND MAGNIFICATION

Matthew R. George
Department of Astronomy, University of California, Berkeley and
Lawrence Berkeley National Laboratory, 1 Cyclotron Road, Berkeley, CA 94720, USA
Draft version August 15, 2013

ABSTRACT

1. INTRODUCTION

We want to measure the shape of the dark matter profile on small scales. This will tell us how baryons have affected the dark matter distribution, the assembly history of the baryons and dark matter as well as feedback processes, and whether dark matter interacts to form "cored" profiles as opposed to the "cuspy" profiles seen in cold dark matter simulations. Measurements of the mass distribution on scales comparable to the effective radius of a galaxy can also constrain the mass-to-light ratio of the stellar population which is uncertain by a factor of ~ 2 depending on the initial mass function which is generally assumed.

Various observational probes have been used to constrain the mass profile of galaxies and dark matter halos, typically with dynamical measurements within a few kpc of the galaxy center, stong lensing arcs a bit farther out, and weak lensing on larger scales to measure the total mass of the halo (e.g., Sand et al. 2004; Koopmans et al. 2006; Gavazzi et al. 2007; Jiang & Kochanek 2007; Auger et al. 2010; Schulz et al. 2010; Newman et al. 2013). While central velocity dispersions or rotation curves can be measured for large samples of galaxies, detailed kinematic measures on scales $\gtrsim 10\,$kpc are difficult and strong lenses exist in only a sparse sample of the galaxy population. Weak lensing, on the other hand, can probe the average profile for large samples of galaxies, allowing studies of population differences and redshift evolution, independent of their dynamical state. For instance, the assembly histories of disk and elliptical galaxies may differ and hydrodynamical simulations predict significant differences in the inner profiles of their dark matter halos. Additionally, weak lensing shear and magnification have different scale-dependence on the surface mass density profile providing added leverage in constraining its shape. The aim of this letter is to investigate how well weak lensing shear and magnification can constrain the inner mass profile of dark matter halos and galaxies.

Several authors have studied the complementarity of shear and magnification, primarily for measuring halo masses (Bartelmann et al. 1996; Bridle et al. 1998; Schneider et al. 2000; van Waerbeke et al. 2010; Rozo & Schmidt 2010; Umetsu et al. 2011) or probing the matter distribution on cosmological scales (van Waerbeke 2010; Casaponsa et al. 2013; Duncan et al. 2013; Krause et al. 2013). Combining shear and magnification increases the statistical precision of a lensing experiment and also enables tests of systematic effects which differ between probes.

While weak lensing experiments traditionally measure galaxy ellipticities to infer the shear signal, magnification can be measured using sizes (Bartelmann & Narayan 1995), fluxes (Broadhurst et al. 1995), or by combining the two (Huff & Graves 2011; Schmidt et al. 2012). Magnification has recently been measured with signal-to-noise approaching that from shear for ensembles of galaxies (Scranton et al. 2005; Hildebrandt et al. 2009; Ménard et al. 2010; Huff & Graves 2011; Ford et al. 2012; Schmidt et al. 2012).

THIS PAPER

We define halos within a virial overdensity of 200 times the critical density of the Universe and use physical distances with $h = 0.7, \Omega_m = 0.3, \Omega_\Lambda = 0.7$.

2. LENS MODELING

The distortion of galaxy images due to weak lensing can be described by a matrix written in terms of the convergence κ and shear components γ_1, γ_2 (e.g. Bartelmann & Schneider 2001):

$$A = \begin{pmatrix} 1-\kappa-\gamma_1 & -\gamma_2 \\ -\gamma_2 & 1-\kappa+\gamma_1 \end{pmatrix}. \quad (1)$$

From galaxy images, one can measure the magnification $\mu = (\det \mathrm{A})^{-1} = [(1-\kappa)^2 - |\gamma|^2]^{-1} \approx 1+2\kappa$ and reduced shear $g = \gamma/(1-\kappa) \approx \gamma$, where we have defined the complex shear $\gamma = \gamma_1 + i\gamma_2$ and approximations are given to first order in the weak limit $|\gamma|, \kappa \ll 1$.

The convergence and tangential component of shear can be related to the projected surface mass density Σ of the lens via

$$\kappa = \frac{\Sigma}{\Sigma_c}; \;\; \gamma_t = \frac{\Delta\Sigma}{\Sigma_c} \quad (2)$$

where the critical surface density Σ_c is a function of the angular diameter distances between the observer (O), lens (L), and source (S),

$$\Sigma_c = \frac{c^2}{4\pi G}\frac{D_{OS}}{D_{OL}D_{LS}}. \quad (3)$$

A typical galaxy lensing experiment averages measurements of g_t or κ in bins of radius R around the lens position to constrain its radial surface density profile (or stacks many such measurements for an ensemble of lenses). Magnification directly probes the surface density at a given position $\Sigma(R)$, whereas shear is sensitive to the excess surface density interior to the projected radius $\Delta\Sigma(R) = \overline{\Sigma}(<R) - \overline{\Sigma}(R)$. This difference in scale-dependence is what we hope to exploit by combining shear and magnification measurements to constrain inner halo profiles.

mgeorge@astro.berkeley.edu

We shall assume that Σ and $\Delta\Sigma$ can be estimated from magnification and shear observables in an unbiased manner down to our minimum radius (typically 40 kpc which is $\sim 20''$ at $z_L = 0.1$). For discussion of modeling lensing observables into the nonlinear regime, see Ménard et al. (2003); Takada & Hamana (2003); Mandelbaum et al. (2006). We will also assume these quantities are constrained independently; see Rozo & Schmidt (2010) for a treatment of their covariance.

We consider parametric models for the three-dimensional density profile $\rho(r)$ of the lens galaxy and dark matter halo, which we then project into two dimensions for comparison with the lensing observables. For the stellar component, we assume a Hernquist (1990) profile of the form

$$\rho_\star(r) = \frac{M_\star}{2\pi}\frac{a}{r(r+r_\star)^3} \quad (4)$$

parametrized by the total stellar mass $M_\star$ and scale radius $r_\star$, which is a good description of elliptical galaxies. If a constant stellar mass-to-light ratio is assumed, the projected scale radius $R_{\rm deV}$ measured from fitting a de Vaucouleurs model to the surface brightness profile of the galaxy can be converted to the three-dimension Hernquist radius using $R_{\rm deV} = 1.8153\, r_\star$. Stellar masses are typically estimated by modeling the spectral energy distribution of a galaxy, but assumptions in this process lead to significant systematic uncertainties dominated by our ignorance of the stellar initial mass function (IMF). We will treat $M_\star$ as a free parameter to see how well lensing can constrain these uncertainties.

Our baseline model for the dark matter halo is the Navarro-Frenk-White (NFW, Navarro et al. 1996) profile with parameters for the halo mass M_h and concentration c. Wright & Brainerd (2000) give projections of this profile to compute $\Sigma_{\rm NFW}$ and $\Delta\Sigma_{\rm NFW}$.

The NFW model was introduced to describe the form of halos in dark matter simulations, but it is known that the baryonic processes including cooling and feedback can modify the shape of the dark matter profile (e.g., Blumenthal et al. 1986; Gao et al. 2004; Gnedin et al. 2004; Johansson et al. 2009; Abadi et al. 2010; Gnedin et al. 2011). Because we lack a good physical description of these processes, we consider a variable amount of halo contraction or expansion using the model of Dutton et al. (2007). This model assumes the quantity $rM(r)^\nu$ is conserved during the formation of a galaxy, with both baryons and dark matter initially distributed following an NFW profile, and the baryons eventually collapsing into a final distribution which we take to be $\rho_\star(r)$ from Equation 4. The parameter ν controls the amount of contraction, with $\nu = 1$ recovering the adiabatic contraction (AC) of Blumenthal et al. (1986), $\nu = 0$ giving an uncontracted NFW profile, and $\nu < 0$ for expansion of the dark matter on small scales. Hydrodynamical simulations predict a range of values $-0.2 \lesssim \nu \lesssim 0.8$ (CHECK?) depending on the details of the cooling and feedback models as well as the assembly history of the galaxy.

We note that these modified halo models are typically implemented assuming that the mass within the virial radius is conserved, i.e., that there is no contraction at or beyond the virial radius. While contraction models produce an excess mass density at $r \lesssim r_\star$, this boundary condition leads to a mass *deficit* on intermediate scales between $\sim r_\star$ and the virial radius, and vice versa for expansion models. We demonstrate this effect in Figure 1 showing ρ, Σ, and $\Delta\Sigma$ halo profiles with model parameters from the faint early-type sample in Table 1 of Schulz et al. (2010). We compare profiles that have undergone expansion ($\nu = -0.2$) or adiabatic contraction to NFW profiles with the same initial halo parameters. To compute the projected profiles we extrapolate $\rho(r)$ from $1-10$ virial radii using the initial NFW profile. The AC model deviates by $\sim 25\%$ from the corresponding NFW model at scales of tens of kiloparsecs. We also see that the shear and magnification observables have different scale-dependence demonstrating their complementarity.

Figure 1 includes a stellar profile for comparison to the halo models. We see that the stars fall off much more rapidly than the dark matter and that the transition between excess and deficit regions for the AC model relative to NFW occurs at roughly the scale where stars and dark matter contribute equally to the total profile. In practice, lensing can only measure the sum of the stellar and dark matter components but we separate these components in the figure to isolate the contraction/expansion effects.

The contraction model depends on the ratios $M_\star/M_h$ and $r_\star/r_h$, with greater contraction for galaxies that are more massive and compact relative to their halos. For a galaxy with $M_\star = 10^{11}\, M_\odot, R_{\rm deV} = 10\,$kpc in a cluster-scale halo with $M_h = 10^{15}\, M_\odot, c = 5$, the AC and expansion models deviate by less than 5% from the NFW profile at $R > 10\,$kpc. The value of $M_\star/M_h$ peaks near $M_\star \approx 10^{10.5}, M_h \approx 10^{12}$ (e.g. Conroy & Wechsler 2009; Behroozi et al. 2010; Leauthaud et al. 2012), which motivates targeting compact galaxies in this mass range, rather than massive clusters or low-mass dwarfs, to measure baryonic contraction effects. Additionally, weak lensing measurements are often limited on small angular scales due to systematic effects, so a low-redshift lens sample allows one to probe smaller physical scales where contraction effects are greatest.

3. FORECASTS

Results. Choice of fiducial system(s) - galaxy vs cluster, concentration, mention miscentering.

Relative S/N of shear vs magnification.

Priors

Plots of constraints.

4. CONCLUSIONS

REFERENCES

Abadi, M. G., Navarro, J. F., Fardal, M., Babul, A., & Steinmetz, M. 2010, MNRAS, 407, 435

Auger, M. W., Treu, T., Bolton, A. S., Gavazzi, R., Koopmans, L. V. E., Marshall, P. J., Moustakas, L. A., & Burles, S. 2010, ApJ, 724, 511

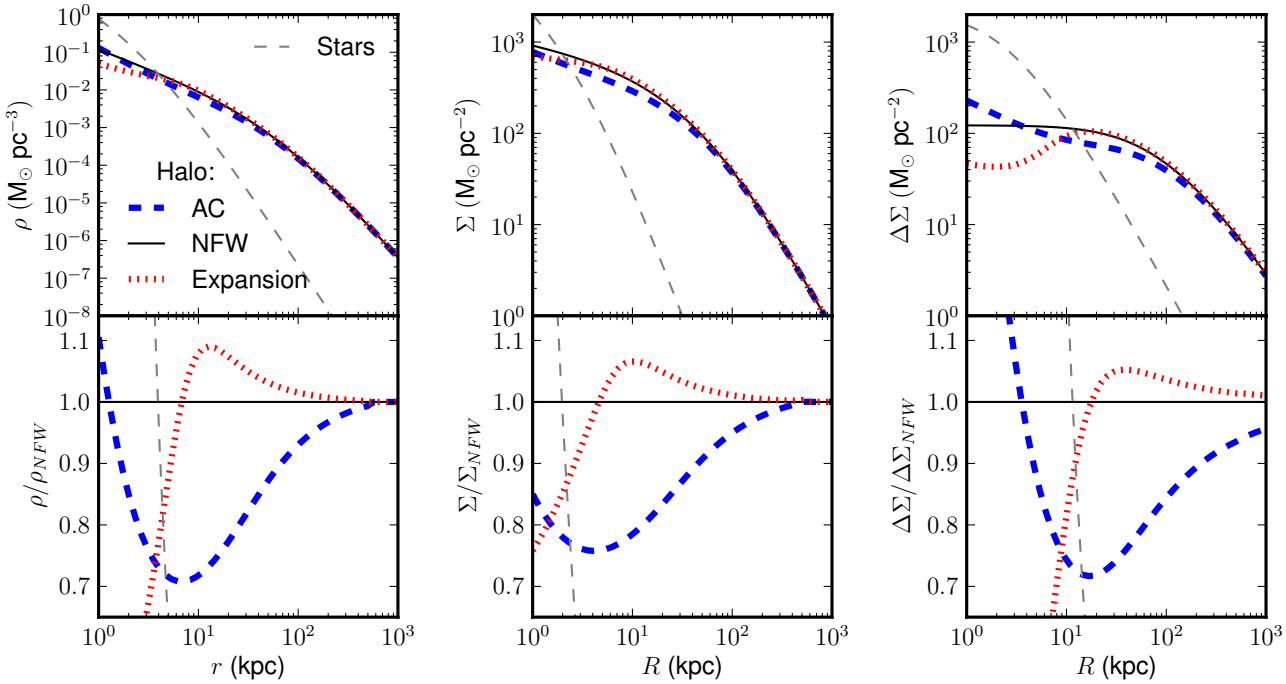

FIG. 1.— Density profiles for different halo models showing the effects of baryonic contraction or expansion relative to NFW. A Hernquist profile for the stellar component is included for comparison. Stellar and NFW model parameters are taken from the faint early-type sample in Table 1 of Schulz et al. (2010): $z = 0.11, M_\star = 7 \times 10^{10}\, M_\odot, M_h = 7 \times 10^{12}\, M_\odot, c = 9, R_{\rm deV} = 3.9\,$kpc (physical). The AC model uses $\nu = 1$ while the Expansion model has $\nu = -0.2$. The boundary condition specifying no contraction at the virial radius leads to a deficit (excess) in the AC (Expansion) profiles relative to NFW at $R_{\rm deV} \lesssim R \lesssim R_{\rm vir}$.

Bartelmann, M., & Narayan, R. 1995, ApJ, 451, 60
Bartelmann, M., Narayan, R., Seitz, S., & Schneider, P. 1996, ApJ, 464, L115
Bartelmann, M., & Schneider, P. 2001, Phys. Rep., 340, 291
Behroozi, P. S., Conroy, C., & Wechsler, R. H. 2010, ApJ, 717, 379
Blumenthal, G. R., Faber, S. M., Flores, R., & Primack, J. R. 1986, ApJ, 301, 27
Bridle, S. L., Hobson, M. P., Lasenby, A. N., & Saunders, R. 1998, MNRAS, 299, 895
Broadhurst, T. J., Taylor, A. N., & Peacock, J. A. 1995, ApJ, 438, 49
Casaponsa, B., Heavens, A. F., Kitching, T. D., Miller, L., Barreiro, R. B., & Martínez-González, E. 2013, MNRAS, 430, 2844
Conroy, C., & Wechsler, R. H. 2009, ApJ, 696, 620
Duncan, C., Joachimi, B., Heavens, A., Heymans, C., & Hildebrandt, H. 2013, ArXiv e-prints
Dutton, A. A., van den Bosch, F. C., Dekel, A., & Courteau, S. 2007, ApJ, 654, 27
Ford, J., et al. 2012, ApJ, 754, 143
Gao, L., Loeb, A., Peebles, P. J. E., White, S. D. M., & Jenkins, A. 2004, ApJ, 614, 17
Gavazzi, R., Treu, T., Rhodes, J. D., Koopmans, L. V. E., Bolton, A. S., Burles, S., Massey, R. J., & Moustakas, L. A. 2007, ApJ, 667, 176
Gnedin, O. Y., Ceverino, D., Gnedin, N. Y., Klypin, A. A., Kravtsov, A. V., Levine, R., Nagai, D., & Yepes, G. 2011, ArXiv e-prints
Gnedin, O. Y., Kravtsov, A. V., Klypin, A. A., & Nagai, D. 2004, ApJ, 616, 16
Hernquist, L. 1990, ApJ, 356, 359
Hildebrandt, H., van Waerbeke, L., & Erben, T. 2009, A&A, 507, 683
Huff, E. M., & Graves, G. J. 2011, ArXiv e-prints
Jiang, G., & Kochanek, C. S. 2007, ApJ, 671, 1568
Johansson, P. H., Naab, T., & Ostriker, J. P. 2009, ApJ, 697, L38
Koopmans, L. V. E., Treu, T., Bolton, A. S., Burles, S., & Moustakas, L. A. 2006, ApJ, 649, 599
Krause, E., Chang, T.-C., Doré, O., & Umetsu, K. 2013, ApJ, 762, L20
Leauthaud, A., et al. 2012, ApJ, 744, 159
Mandelbaum, R., Seljak, U., Cool, R. J., Blanton, M., Hirata, C. M., & Brinkmann, J. 2006, MNRAS, 372, 758
Ménard, B., Hamana, T., Bartelmann, M., & Yoshida, N. 2003, A&A, 403, 817
Ménard, B., Scranton, R., Fukugita, M., & Richards, G. 2010, MNRAS, 405, 1025
Navarro, J. F., Frenk, C. S., & White, S. D. M. 1996, ApJ, 462, 563
Newman, A. B., Treu, T., Ellis, R. S., Sand, D. J., Nipoti, C., Richard, J., & Jullo, E. 2013, ApJ, 765, 24
Rozo, E., & Schmidt, F. 2010, ArXiv e-prints
Sand, D. J., Treu, T., Smith, G. P., & Ellis, R. S. 2004, ApJ, 604, 88
Schmidt, F., Leauthaud, A., Massey, R., Rhodes, J., George, M. R., Koekemoer, A. M., Finoguenov, A., & Tanaka, M. 2012, ApJ, 744, L22
Schneider, P., King, L., & Erben, T. 2000, A&A, 353, 41
Schulz, A. E., Mandelbaum, R., & Padmanabhan, N. 2010, MNRAS, 408, 1463
Scranton, R., et al. 2005, ApJ, 633, 589
Takada, M., & Hamana, T. 2003, MNRAS, 346, 949
Umetsu, K., Broadhurst, T., Zitrin, A., Medezinski, E., & Hsu, L.-Y. 2011, ApJ, 729, 127
van Waerbeke, L. 2010, MNRAS, 401, 2093
van Waerbeke, L., Hildebrandt, H., Ford, J., & Milkeraitis, M. 2010, ApJ, 723, L13
Wright, C. O., & Brainerd, T. G. 2000, ApJ, 534, 34